Title

Bryostatin 1 Promotes Synaptogenesis and Reduces Dendritic Spine Density in Cortical Cultures through a PKC-Dependent Mechanism

Journal

ACS Chemical Neuroscience, 11(11)

ISSN

1948-7193

Authors

Ly, Calvin
Shimizu, Akira J
Vargas, Maxemiliano V
et al.

Publication Date

2020-06-03

DOI

10.1021/acschemneuro.0c00175

Peer reviewed

Published in final edited form as:

ACS Chem Neurosci. 2020 June 03; 11(11): 1545–1554. doi:10.1021/acschemneuro.0c00175.

Bryostatin 1 Promotes Synaptogenesis and Reduces Dendritic Spine Density in Cortical Cultures through a PKC-Dependent Mechanism.

Calvin Ly[1], **Akira J. Shimizu**[2], **Maxemiliano V. Vargas**[3], **Whitney C. Duim**[1], **Paul A. Wender**[2,4], **David E. Olson**[1,5,6,*]

[1]Department of Chemistry, University of California, Davis, One Shields Avenue, Davis, California 95616, USA

[2]Department of Chemistry, Stanford University, 333 Campus Drive, Stanford, CA 94305, USA

[3]Neuroscience Graduate Program, University of California, Davis, 1544 Newton Ct, Davis, California 95618, USA

[4]Chemical and Systems Biology, Stanford University, 269 Campus Drive, Stanford, CA 94305, USA

[5]Department of Biochemistry & Molecular Medicine, School of Medicine, University of California, Davis, 2700 Stockton Blvd, Suite 2102, Sacramento, California 95817, USA

[6]Center for Neuroscience, University of California, Davis, 1544 Newton Ct, Davis, California 95618, USA

Abstract

The marine natural product bryostatin 1 has demonstrated procognitive and antidepressant effects in animals and has been entered into human clinical trials for treating Alzheimer's disease (AD). The ability of bryostatin 1 to enhance learning and memory has largely been attributed to its effects on the structure and function of hippocampal neurons. However, relatively little is known about how bryostatin 1 influences the morphology of cortical neurons—key cells that also support learning and memory processes and are negatively impacted in AD. Here, we use a combination of carefully designed chemical probes and pharmacological inhibitors to establish that bryostatin 1 increases cortical synaptogenesis while decreasing dendritic spine density in a protein kinase C (PKC)-dependent manner. The effects of bryostatin 1 on cortical neurons are distinct from those induced by neural plasticity-promoting psychoplastogens such as ketamine. Compounds capable

*Corresponding Author: deolson@ucdavis.edu.

Author Contributions

DEO and PAW conceived the project. DEO and CL were responsible for the overall experimental design with input from PAW and AJS. CL performed the synaptogenesis experiments. AJS synthesized and characterized some of the chemical tools used in this study and evaluated their PKC binding. MVV performed the dendritogenesis assay. WCD performed the dendritic spine experiments with assistance from CL. DEO wrote the manuscript with input from all authors.

Conflict of Interest

DEO is the president and chief scientific officer of Delix Therapeutics, Inc. Stanford University has filed patent applications on this and related technology, which has been licensed by Neurotrope BioScience for the treatment of neurological disorders and by Bryologyx Inc. for use in HIV/AIDS eradication and cancer immunotherapy. PAW is an advisor to both companies and a cofounder of the latter.

of increasing synaptic density with concomitant loss of immature dendritic spines may represent a unique pharmacological strategy for enhancing memory by improving signal-to-noise ratio in the central nervous system.

Graphical Abstract

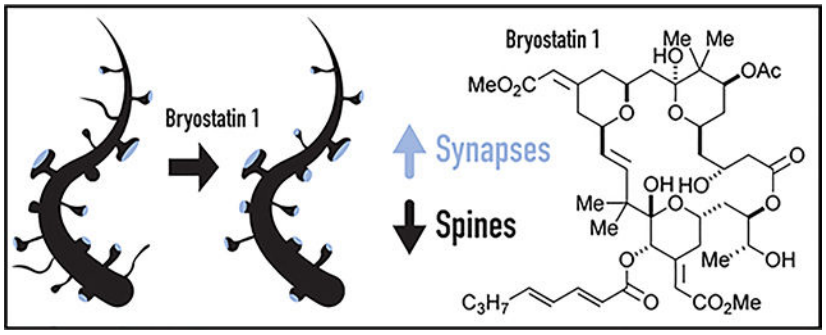

Keywords

bryostatin 1; Alzheimer’s disease; synaptogenesis; dendritic spines; protein kinase C (PKC)

INTRODUCTION

Alzheimer’s disease (AD) and related dementias affected 1.6% of the United States population in 2014[1] and are among the leading causes of death and disability worldwide.[2] As the global population continues to age, the need for identifying effective medicines to treat AD is intensifying. Thus far, therapeutic approaches focusing solely on eliminating the pathological hallmarks of the disease (e.g., amyloid plaques and neurofibrillary tangles) have largely failed.[3] Therefore, strategies directly addressing cognitive impairment and synapse loss while simultaneously reducing the accumulation of toxic misfolded proteins have enormous potential.

The protein kinase C (PKC) family of proteins is well known to be involved in both memory formation and the regulation of misfolded proteins characteristic of AD. There are 12 isoforms of PKC in mammals, with many being highly expressed in the brain.[4] Due to the roles that PKCα, PKCγ, PKCε, and PKCζ play in the cellular mechanisms that underly learning and memory, they are sometimes referred to as “memory kinases.”[4] In addition to their essential roles in normal brain function, these kinases are also involved in pathological states such as AD. For example, amyloid β-peptide (Aβ) downregulates PKC levels[5] and can directly inhibit PKCα and PKCε.[6] Moreover, PKC is known to decrease Aβ formation[7] and promote Aβ clearance.[8] Therefore, activators of PKC might prove therapeutic for treating AD and related disorders.[9]

The phorbol esters, including phorbol 12-myristate 13-acetate (PMA), are some of the most well-known activators of PKC (Figure 1). In fact, these compounds have been shown to potently potentiate synaptic transmission in the hippocampus.[10,11] However, the well-known cancer promoting properties of several phorbol esters have drastically limited their

therapeutic potential.[12,13] Unlike these compounds, the marine natural product bryostatin 1 (BRYO) does not promote tumor formation[12,14] despite the fact that it is a potent modulator of several PKC isozymes (Figure 1).[15] This macrocylic lactone was originally isolated from *Bugula neritina* by Pettit and co-workers[16] and has demonstrated impressive effects on neuronal structure and function. BRYO increases both transcript and proteins levels of brain-derived neurotrophic factor (BDNF) in the hippocampus[17] and facilitates hippocampal long-term potentiation.[18] Additionally, BRYO increases hippocampal dendritic spine density in aged rats,[19] promotes mushroom spine growth when administered in combination with Morris Water Maze (MWM) training,[20] and rescues spine and synapse loss in two AD mouse models (Tg2576 and 5XFAD transgenic mice).[21]

Changes in dendritic spine and synapse density are believed to underly the pro-cognitive effects of BRYO. Intracerebroventricular (ICV) administration of BRYO has been shown to enhance memory in the MWM paradigm,[24] and rescues spatial learning and memory deficits exhibited by several rodent models of brain disorders including fragile X syndrome[17,25] and ischemic stroke.[26,27] In transgenic rodent models of AD, BRYO not only improved memory, [21] it also reduced levels of Aβ40 and Aβ42 while decreasing mortality rates in male mice.[28] Owing to its promising effects in animal models, BRYO entered clinical trials for treating AD.[29,30] The supply of this structurally complex natural product has been an issue due to its low and variable natural abundance, environmental and cost issues associated with harvesting the marine organism, and the formidable challenges associated with its synthesis. Fortunately, the Wender group has recently reported a scalable synthesis that supplies sufficient quantities of BRYO and its analogs for future research and clinical development.[31]

Despite early signs of success in mouse models of brain disorders, BRYO is very large (MW = 905.03 g/mol) and does not possess the physicochemical properties typically associated with most successful CNS therapeutics.[32] While it can cross the blood-brain barrier (BBB),33 its peak concentration (C_{max}) is quite low (200 pM in mice).[34] In this respect, simplified and tunable bryostatin analogs (i.e., bryologs) could prove extremely useful. [35,36,37,38,39,40,41,42,43] Additionally, these analogs can serve as powerful chemical tools for investigating bryostatin's mechanism of action. Here, we use a combination of pharmacological tools, including bryostatin and prostratin analogs, to demonstrate that BRYO increases cortical synaptogenesis and decreases cortical spinogenesis through a PKC-dependent mechanism. To date, nearly all mechanistic work on BRYO has focused on its effects on hippocampal neurons. Our study is directed at understanding how this important natural product, its analogs, and other PKC modulators impact the structure of cortical neurons—key players in learning, memory, and the pathophysiology of AD.

To determine the effects of BRYO on cortical synaptogenesis, we treated rat embryonic cortical cultures with varying concentrations of BRYO for either 15 min, 6 h, or 24 h, and performed immunocytochemistry experiments to visualize both pre- (VGLUT1) and postsynaptic (PSD-95) markers (Figure 2). Synapse density was determined via co-localization of VGLUT1 and PSD-95 puncta. By employing threshold cutoffs (see Methods) and restricting the size of colocalization events to < 1.5 μm (approximately the size of a large mushroom spine),[44] we were able to eliminate artifacts and the majority of nonsynaptic colocalization events (e.g, large areas of colocalization on the soma). Similar

approaches for the immunocytochemical detection of synapses have been reported previously.[45,46,47,48,49,50] Because it is high-throughput, immunocytochemistry has become the preferred method for quantifying synapse density as part of phenotypic drug screening campaigns. Despite lacking resolution, quantification of synapse density using traditional fluorescence microscopy correlates exceptionally well with ultrastructural techniques such as electron microscopy and super-resolution imaging.[51,52,53]

We found that BRYO had little to no effect on VGLUT1 density; however, PSD-95 density and synapse density both increased with inverted U-shaped concentration and time responses (Figure 2A and B). Synapse density increased to a greater extent than did PSD-95 density (Figure 2B), indicating that BRYO-induced synaptogenesis cannot be solely explained by an upregulation of PSD-95 leading to coincidental colocalization with presynaptic puncta. Overexpression of PSD-95 is known to cause the maturation of glutamatergic presynaptic terminals,[54] which could account for the increase in synapse density observed after BRYO treatment.

The inverted U-shaped concentration and time responses observed following BRYO treatment were quite obvious. BRYO has previously been shown to produce biphasic concentration responses in other biological assays involving PKC,[55,56] likely due to its ability to down-regulate PKC via ubiquitination when treated at high concentrations or for prolonged periods of time.[57,58] Therefore, we next attempted to determine if BRYO increases cortical synapse density through a PKC-dependent mechanism. A 10 nM treatment of BRYO for 6 h produced the maximal increase in synapse density. Based on the K_i values of BRYO (Figure 1B), a 10 nM concentration would be predicted to activate various PKC isoforms, and thus, this concentration and time point were used for all subsequent experiments. Like BRYO, the compounds BA **1**, PMA, and PA **3** are known to bind conventional and novel PKC isoforms with nanomolar affinities (Figure 1).[22,40,59,60,61] All four of these compounds increased cortical synaptic density when treated at 10 nM for 6h to a comparable extent as ketamine (10 μM)—a well-known psychoplastogen[62] and fast-acting antidepressant (Figure 3A and B). Pre- and postsynaptic colocalizations (i.e., synapses) were observed primarily on or directly adjacent to dendritic shafts. The fact that multiple PKC modulators from two distinct chemical scaffolds (bryostatin and phorbol) produced similar results on cortical synaptogenesis increased our confidence that PKC plays a key role in their mechanisms of action. Furthermore, previous work has demonstrated that PKC activators increase PSD-95 membrane localization through direct phosphorylation of serine 295 in human hippocampal neurons.[63]

To ensure that the synaptogenic effects of BRYO, BA **1**, PMA, and PA **3**, were not simply the result of off-target effects due to the unique properties of the bryostatin and phorbol scaffolds, we employed compounds IBA **2** and IPA **4**—PKC-inactive structural analogs of BRYO and prostratin, respectively (Figure 1).[64,65] Previously, we have shown that structurally similar negative control compounds can be extremely useful for identifying off-target mechanisms of action.[42,66,67] In this case, neither IBA **2** nor IPA **4** were able to promote synaptogenesis (Figure 3A and B), strongly implicating PKC in the synaptogenic mechanism of BRYO and phorbol esters. This conclusion was further supported by treatment with the PKC inhibitor Gö 6983,[68] which blocked the effects of BRYO and BA **1**

(Figure 3C), consistent with our hypothesis that PKC plays an essential role in promoting synaptogenesis in cortical cultures following treatment with BRYO.

As increased cortical synapse density following treatment with PKC modulators mirrored increased PSD-95 density, we were interested to determine the effects of BRYO on dendritic spines. Dendritic spines are critical post-synaptic structures where the majority of PSD-95 is localized, and thus, we hypothesized that BRYO would increase dendritic spine density. However, we were surprised to observe that treatment of cortical neurons with BRYO led to a marked reduction in dendritic spine density (Figure 4). Because PKC is known to play a critical role in regulating the dynamics of the actin cytoskeleton,[69] we next determined the role of this kinase in the effects of BRYO on spine density. As expected, BRYO-induced spine loss was blocked by Gö 6983, and the PKC-inactive compound IBA **2** did not produce this phenotype (Figure 4B). Bryostatin induced a greater reduction in filopodia than mushroom spine density (Figure 4C).

Recently, Margolis and co-workers observed that overexpression of PKCα or PKCε in cultured hippocampal neurons reduced dendritic spine density at 12 days in vitro (DIV12).[70] Moreover, they demonstrated that treatment with BRYO led to a reduction in dendritic spine density in immature hippocampal cultures (DIV12), but that more mature hippocampal neurons (DIV18) were resilient to BRYO-induced spine loss.[70] In contrast, we observe that BRYO is capable of reducing spine density even on mature cortical neurons (DIV20) (Figure 4).

Changes in dendritic spine density are often correlated with changes in dendritic arbor complexity.[62,71] However, overexpression of several PKC isoforms is known to enhance the dendritic branching of hippocampal neurons,[70] and therefore, it was unclear to us if treatment with BRYO would have a positive or negative impact on the dendritic growth of cortical neurons. Surprisingly, treatment of cortical cultures with compounds BRYO, BA **1**, IBA **2**, PMA, PA **3**, or IPA **4** did not change dendritic arbor complexity as measured by Sholl analysis (Figure 5). This result contrasts sharply with the effects of ketamine (Figure 5), suggesting that the antidepressant effects of BRYO[24] are unlikely due to changes in cortical structural plasticity as has been proposed for ketamine[72,73] and other psychoplastogens.[71] Instead, they likely arise from increased synaptogenesis in hippocampal and/or cortical regions.

Using a combination of chemical tools, we were able to demonstrate for the first time that the PKC modulator BRYO increases cortical synaptogenesis while decreasing cortical spine density via PKC-dependent mechanisms. Future electrophysiology experiments will be important for understanding how these structural changes impact neuronal function. Additionally, our study highlights both similarities and differences between the effects of BRYO on cortical and hippocampal neurons. For example, BRYO decrease spine density on both cortical and hippocampal neurons; however, mature cortical neurons appear to be more sensitive than mature hippocampal neurons to BRYO-induced spine loss.

Taken together, our results suggest that BRYO and associated PKC-activating analogs produce changes in cortical structural plasticity that are completely distinct from those

induced by psychoplastogens. BRYO does not enhance dendritic branching, and instead causes dendritic spine loss with concomitant increases in synaptic density. This very unique, chemically induced phenotype has the potential to improve cortical communication by enhancing the signal-to-noise ratio. In support of this hypothesis, BRYO has been shown to reduce the density of immature hippocampal spines in a mouse model of fragile X syndrome and rectify the associated cognitive deficits.[17,25] It is quite possible that the combination of increasing synaptic density while decreasing immature dendritic spine density could underly the promising effects of BRYO for improving memory and treating AD. The current lack of effective medicines for treating neuropsychiatric and neurodegenerative diseases underscores our desperate need to identify neurotherapeutics with novel mechanisms of action. Harnessing the unique type of induced neural plasticity (iPlasticity)[74] promoted by BRYO and other PKC modulators may prove useful for treating disorders characterized by impaired memory and cognitive function.

METHODS

Drugs

Bryostatin 1 and all associated bryostatin and prostratin analogs were synthesized by Professor Paul Wender's group at Stanford University. PMA is commercially available. Compounds were stored as 10 mM DMSO stock solutions under nitrogen. Stock solutions were diluted in media to final concentrations of 0.1% or 0.2% DMSO for single treatments and inhibitor studies, respectively. Ketamine hydrochloride (Fagron) and Gö 6983 (Tocris, 2285) were purchased from commercial sources.

Animals

Sprague-Dawley rats were obtained from Charles River Laboratories (Wilmington, MA, USA). All experimental procedures involving animals were approved by the University of California, Davis Institutional Animal Care and Use Committee (IACUC) and adhered to the principles described in the NIH Guide for the Care and Use of Laboratory Animals. The University of California, Davis is accredited by the Association for Assessment and Accreditation of Laboratory Animal Care International (AAALAC).

PKC Binding Assay

The protein kinase C (PKC) affinities of bryostatin 1 and analog compounds were determined via competition with ^{3}H-phorbol-12,13-dibutyrate (^{3}H-PDBu) as described below. This procedure entails a glass-fiber filtration method to determine bound radioligand. First, to a 50 mL polypropylene tube was added Tris-HCl (pH 7.4, 1 M, 1 mL), KCl (1 M, 2 mL), $CaCl_2$ (0.1 M, 30 μL), and bovine serum albumin (40 mg, Sigma-Aldrich). This mixture was diluted to 20 mL with deionized H_2O and mixed gently. The PKC assay buffer was stored on ice until use. For every two assays, 3.5 mg phosphatidylserine (PS) (Avanti Polar Lipids, porcine, 25 mg/mL $CHCl_3$ solution) was concentrated by remo›ving chloroform under a stream of nitrogen followed by reduced pressure. The solid PS was suspended as vesicles in freshly prepared PKC binding assay buffer (3.5 mL) by sonicating six times for 30 s, with a 30 s rest between sonications (Branson Sonifier 250, power = 2, 50% duty cycle). The resulting milky cloudy mixture (1 mg/mL) was stored on ice until use.

Next, a 4 μg aliquot of the indicated recombinant human PKC isoform (Invitrogen) was dissolved in 11.6 mL of PKC binding assay buffer (this amount is sufficient for two assays). The diluted PKC was stored on ice for immediate use. To prepare a solution of the radioligand, ^{3}H-PDBu (American Radiolabeled Chemicals, Inc.; 1 mCi/mL acetone solution; specific activity: 20 Ci/mmol) was diluted 10-fold with DMSO. The resulting 500 nM stock solution was further diluted with DMSO to 30 nM. Compound solutions were prepared through serial dilution from a chosen "high" concentration by factors of 3 or 4. For each analog compound, seven concentrations were used to define the inhibition curve. To prepare the Master Mix solution, 3.3 mL of 1 mg/mL PS vesicles solution, 11 mL of PKC isoform solution, and 1.1 mL of 30 nM ^{3}H-PDBu solution were added to a polypropylene tube. The resulting Master Mix was vortexed and stored on ice. Prior to performing the assay, glass-fiber filters (Whatman GF/B) were prepared by soaking in a solution of aqueous polyethyleneimine (10% by vol, 18 mL) in DI H_2O (600 mL) for ≥1h. Additionally, 500 mL rinsing buffer was prepared (20 mM Tris, pH 7.4) and cooled on ice for the duration of the incubation period and for the remainder of the assay. The assay was run in triplicate for each analog concentration. For each data point, 280 μL of Master Mix solution and 20 μL of compound at a specified concentration were added to a polypropylene tube. Non-specific ^{3}H-PDBu binding was assessed in triplicate by substitution of the analog compound with unlabeled PDBu (20 μL of a 75 μM stock, assay concentration: 5 μM). Maximal ^{3}H-PDBu binding was assessed in triplicate by substitution of the analog compound with 20 μL DMSO. The solutions were vortexed to mix, incubated at 37 °C for 10 min, and incubated on ice for at least 30 min prior to filtration. Using a Brandel Harvester, the assay contents from each polypropylene tube were vacuum-filtered through polyethylenimine-soaked filters, washing with rinsing buffer (3X) and drying first under vacuum for 5 min and then under ambient conditions for ≥ 2h. The resulting filters had circular perforations for each data point, which were removed with forceps and placed in a scintillation vial. Scintillation vials were filled with Bio-Safe II scintillation fluid (5 mL) and measured for radioactivity using a Beckman LS 6500SC scintillation counter. Counts per minute (cpm) were averaged for each triplicate dilution. The data were plotted – cpm vs. log(concentration) – using Graphpad Prism Software and an IC_{50} was determined using that program's built-in one-site competition least squares regression function. K_i values were calculated using the equation: $K_i = IC_{50} / (1 + ([^{3}\text{H-PDBu}] / K_d))$, with the free concentration of ^{3}H-PDBu being assumed to be nearly equal to the added concentration (i.e., 2 nM). The K_d of ^{3}H-PDBu was measured via saturation binding under identical conditions (α = 15.1 nM, βI = 8.8 nM, γ = 13.8 nM, δ = 4.5 nM, ε = 6.2 nM, η = 18.4 nM, θ = 28.8 nM.

Cell Culture

Primary cortical cell cultures were prepared as described previously.[71] Briefly, pregnant Sprague-Dawley dams were euthanized at embryonic day 18 (E18), and the cortices of the pups were harvested. Cells were plated on poly-D-lysine coated plates at specific densities depending on the experiment (vide infra). Cultures were maintained at 37ºC under an atmosphere containing 5% CO_2. Plating media consisted of 10% heat-inactivated fetal bovine serum (FBS; Life Technologies), 1% penicillin-streptomycin (Life Technologies), and 0.5 mM glutamine (Life Technologies) in Neurobasal (Life Technologies). After 16–24 h, media was exchanged for replacement media consisting of 1× B27 supplement (Life

Technologies), 1% penicillin-streptomycin, 0.5 mM glutamine, and 12.5 μM glutamate in Neurobasal. For experiments requiring cells older than 7 days in vitro (DIV7), at 96 h post-plating, 50% of media was removed and feeding media containing 1× B27 supplement, 1% penicillin-streptomycin, 0.5 mM glutamine in Neurobasal was added with an additional 20% volume added to account for evaporation.

Synaptogenesis Experiments

Synaptogenesis experiments were performed using 96-well plates coated with poly-D-lysine at a density of 15,000 cells per well. The outer wells were not used to avoid edge effects. An 8-point concentration response (10 μM to 1 pM) at 3 time points (15 min, 6 h, and 24 h) was conducted for bryostatin 1. Cells were challenged with drugs on DIV19 (24 hour treatment) or DIV20 (15 minutes and 6 hours). Studies with the bryostatin analogs were performed using a concentration of 10 nM for 6 h on DIV20. For inhibitor studies, cells were pretreated with Gö 6983 (100 nM) for 10 min prior to the addition of compounds (10 nM). At the completion of the treatment period, 80% of the media was removed and a 50% volume of a 4% aqueous paraformaldehyde (PFA) solution at room temperature was added. The fixative was applied to the cultures for 20 min at room temperature. Cells were then washed two times with Dulbecco's phosphate-buffered saline (dPBS, Life Technologies). For immunocytochemistry experiments, cells were permeabilized with 0.2% Triton X-100 (ThermoFisher, 85111) in dPBS for 20 min at room temperature without shaking. Plates were then blocked with antibody diluting buffer (ADB) containing 2% bovine serum albumin (BSA) in dPBS for 1 h at room temperature without shaking. Then, plates were incubated overnight at 4°C with gently shaking in ADB and a chicken anti-MAP2 antibody (1:10,000; EnCor, CPCA-MAP2), a guinea pig anti-vGLUT1 antibody (1:1000; Millipore, AB5905, validated using genetic knockout[75]), and a mouse anti-PSD-95 antibody (1:500; Millipore, MABN68, validated using shRNA knockdown[76]). The next day, plates were washed three times in dPBS and once in ADB. Plates were then incubated in ADB at room temperature containing an anti-chicken IgG secondary antibody conjugated to Alexa Fluor 488 (1:500; LifeTechnologies), an anti-guinea pig IgG secondary antibody conjugated to Cy3 (1:500; Jackson ImmunoResearch Inc., 706–165-148), and an anti-mouse IgG secondary antibody conjugated to Cy5 (1:500; Jackson ImmunoResearch Inc., 715–605-151) for 1 h. Next, plates were washed five times with dPBS and after the final wash, 100 μL of dPBS was added to each well. All images were obtained using a Molecular Devices ImageXpress Micro XLS Widefield High-Content Analysis System at 9 sites per well using 40× magnification.

Analysis was done using MetaXpress software. To quantify pre- and postsynaptic densities, the "Find Round Object" feature was used to produce a mask on both the vGLUT1 (presynaptic mask) and PSD-95 (postsynaptic mask) channels. The longest diameter of the objects was restricted to a range from 0.5 μm to 1.5 μm with intensities greater than 2500 unit and 1500 unit compared to the background for vGLUT1 and PSD-95, respectively. Then, the program created a mask using the MAP2 channel, restricting the mask to 0 μm to 30 μm and an intensity of greater than 1,000 compared to the background. The number of events occurring in either the presynaptic mask or the postsynaptic mask was quantified and these values were normalized to the measured MAP2 channel mask area (number of counts

per um^2). Normalized data were then tested for outliers using the ROUT method in Graphpad Prism (version 8) at a Q = 1%. The outlier test was completed to remove artifacts in an unbiased manner.

To measure synaptic density, the presynaptic and postsynaptic masks were overlaid using the logical operation “and” to retain only signal that colocalized to form the synapse mask. The number of events occurring in this synapse mask was quantified and normalized to the MAP2 channel mask area (number of counts per um^2). Normalized data were then tested for outliers using the ROUT method in Graphpad Prism (version 8) at a Q = 1%. The outlier test was completed to remove artifacts in an unbiased manner.

Spinogenesis Experiments

Cells were plated at a density of 35,000 cells per well onto poly-D-lysine coated coverslips in 24 well plates and subjected to treatments on DIV20. For antagonist studies, cells were pretreated with Gö 6983 (100 nM) or vehicle (0.1% DMSO) 10 min prior to the start of the experiment. Cells were treated with drugs or vehicle (final concentration of 0.2% DMSO) for 6 h total. Next, 80% of the media was removed and a 50% volume of a 4% aqueous PFA solution at room temperature was added. The plate was incubated for 20 minutes at room temperature. Cells were washed two times with dPBS and permeabilized with 0.2% Triton X-100 in dPBS for 20 minutes at room temperature without shaking. Plates were then blocked with ADB containing 2% BSA in dPBS for 1 hour at room temperature without shaking. Next, plates were incubated overnight at 4°C with gently shaking in ADB containing a chicken anti-MAP2 antibody (1:10,000; EnCor, CPCA-MAP2). The next day, plates were washed three times with dPBS and once with ADB. Plates were then incubated in ADB at room temperature containing an anti-chicken IgG secondary antibody conjugated to Alexa Fluor 405 (1:500; AbCam, ab175675) and phalloidin conjugated to Alexa Fluor 488 (1:40; Thermofisher, A12379) for 1 hour. Following this, the plates were washed five times with dPBS and after the final wash, dPBS (500 μL) was added to each well. Coverslips were then mounted onto microscope slides with ProLong Gold (Life Technologies, P36930), allowed to cure at room temperature for 24 hours, and sealed using nail polish. Images were taken on a Nikon High Content Analysis Spinning Disk Confocal Microscope at 100X. Dendritic spines were manually counted by an experimenter blinded to treatment condition. Spines were counted on secondary dendritic branches of similar thickness that were located away from other dendrites/somas and clear of debris. Spines were visually defined as one of the following spine types: filopodia, thin, stubby, and mushroom. Filopodia spines were defined as having a long, thin f-actin signal lacking a spine head. Thin spines were defined as having an f-actin spine neck leading to a small spine head. Stubby spines lacked spine necks and were defined as concentrated f-actin signals (almost like punctate) localized on or directly adjacent to a dendritic shaft. Mushroom spines were defined as spines having a short spine neck and large spine head (i.e., mushroom shaped). Finally, the number of dendritic spine was normalized to the length of dendrite.

Dendritogenesis Experiments

Dendritogenesis experiments were performed using 96-well plates coated with poly-D-lysine at a density of 15,000 cells per well. The outer wells were not used to avoid edge

effects. Cultures were treated on DIV3 compounds or vehicle for 1 hour at 10 nM. Ketamine (10 μM) was used as a positive control. After 1 h, the media was replaced with fresh replacement media, and the cultures were allowed to continue to grow for an additional 71 h. Next, 80% of the media was removed and a 50% volume of a 4% aqueous PFA solution at room temperature was added. The plate was incubated for 20 minutes at room temperature. Cells were washed two times with dPBS and permeabilized with 0.2% Triton X-100 in dPBS for 20 minutes at room temperature without shaking. Plates were then blocked with ADB containing 2% BSA in dPBS for 1 hour at room temperature without shaking. Next, the plates were incubated overnight at 4°C with gently shaking in ADB containing a chicken anti-MAP2 antibody (1:10,000; EnCor, CPCA-MAP2). The following day, the plates were washed three times with dPBS and once with ADB. Plates were then incubated in ADB at room temperature containing an anti-chicken IgG secondary antibody conjugated to Alexa Fluor 488 (1:500; LifeTechnologies) for 1 h. Next, plates were washed five times with dPBS and after the final wash, 100 μL of dPBS was added to each well. Images were taken using a Molecular Devices ImageXpress Micro XLS Widefield High-Content Analysis System at 9 sites per well using 20× magnification. Images were quantified in ImageJ Fiji (version 1.52i) using the Sholl Analysis Plug-in as described previously.[77]

Data Analysis and Statistics.

Treatments were randomized, and data were analyzed by experimenters blinded to treatment conditions. Statistical analyses were performed using GraphPad Prism (version 8.1.2). All comparisons were planned prior to performing each experiment. Data are represented as mean ± SEM, unless otherwise noted, with asterisks indicating *$p < 0.05$, **$p < 0.01$, ***$p < 0.001$, and ****$p < 0.0001$.

Acknowledgement

This work was supported by funds from the National Institutes of Health (NIH) (R01GM128997 to DEO, R01CA31845 to PAW) and two NIH training grants (T32GM113770 to CL and 5T32GM099608 to MV). This project used the Biological Analysis Core of the UC Davis MIND Institute Intellectual and Development Disabilities Research Center (U54 HD079125) and the Nikon high content analysis spinning disk confocal microscope (1S10OD019980–01A1) in the Light Microscopy Imaging Facility in the Department of Molecular and Cellular Biology at UC Davis. We thank Daryl Staveness, Jack Sloane, and Katie Near for synthesizing the inactive bryostatin and prostratin analogs.

REFERENCES

1. Matthews KA; Xu W; Gaglioti AH; Holt JB; Croft JB; Mack D; McGuire LC Racial and ethnic estimates of Alzheimer's disease and related dementias in the United States (2015–2060) in adults aged ≥65 years. Alzheimers Dement., 2019, 15, 17–24. [PubMed: 30243772]
2. GBD 2016 Neurology Collaborators. Global, regional, and national burden of neurological disorders, 1990–2016: a systematic analysis for the Global Burden of Disease Study 2016. Lancet Neurol, 2019, 18, 459–480. [PubMed: 30879893]
3. Madav Y; Wairkar S; Prabhakar B Recent therapeutic strategies targeting beta amyloid and tauopathies in Alzheimer's disease. Brain Res. Bull, 2019, 146, 171–184. [PubMed: 30634016]
4. Sun MK; Alkon DL The "memory kinases": roles of PKC isoforms in signal processing and memory formation. Prog. Mol. Biol. Transl. Sci, 2014, 122, 31–59. [PubMed: 24484697]
5. Pakaski M; Balaspiri L; Checler F; Kasa P Human amyloid-beta causes changes in the levels of endothelial protein kinase C and its alpha isoform in vitro. Neurochem. Int, 2002, 41, 409–414. [PubMed: 12213228]

6. Lee W; Boo JH; Jung MW; Park SD; Kim YH; Kim SU; Mook-Jung I Amyloid beta peptide directly inhibits PKC activation. Mol. Cell. Neurosci, 2004, 26, 222–331. [PubMed: 15207847]
7. Desdouits F; Buxbaum JD; Desdouits-Magnen J; Nairn AC; Greengard P Amyloid beta peptide formation in cell-free preparations. Regulation by protein kinase C, calmodulin, and calcineurin. J. Biol. Chem, 1996, 271, 24670–24674. [PubMed: 8798734]
8. Choi DS; Wang D; Yu GQ; Zhu G; Kharazia VN; Paredes JP; Chang WS; Deitchman JK; Mucke L; Messing RO PKC epsilon increases endothelin converting enzyme activity and reduces amyloid plaque pathology in transgenic mice. Proc. Natl. Acad. Sci. USA, 2006, 103, 8215–8220. [PubMed: 16698938]
9. Sun MK; Alkon DL Protein kinase C activators as synaptogenic and memory therapeutics. Arch. Pharm. (Weinheim), 2009, 342, 689–698. [PubMed: 19899099]
10. Malenka RC; Madison DV; Nicoll RA Potentiation of synaptic transmission in the hippocampus by phorbol esters. Nature, 1986, 321, 175–177. [PubMed: 3010137]
11. Malinow R; Madison DV; Tsien RW Persistent protein kinase activity underlying long-term potentiation. Nature, 1988, 335, 820–824. [PubMed: 2847049]
12. Nelson TJ; Alkon DL Neuroprotective versus tumorigenic protein kinase C activators. Trends Biochem. Sci, 2009, 34, 136–145. [PubMed: 19233655]
13. Blumberg PM Protein kinase C as the receptor for the phorbol ester tumor promoters: sixth Rhoads memorial award lecture. Cancer Res, 1988, 48, 1–8. [PubMed: 3275491]
14. Hennings H; Blumberg PM; Pettit GR; Herald CL; Shores R; Yuspa SH Bryostatin 1, an activator of protein kinase C, inhibits tumor promotion by phorbol esters in SENCAR mouse skin. Carcinogenesis, 1987, 8, 1343–1346. [PubMed: 3621472]
15. Szallasi Z; Smith CB; Pettit GR; Blumberg PM Differential regulation of protein kinase C isozymes by bryostatin 1 and phorbol 12-myristate 13-acetate in NIH 3T3 fibroblasts. J. Biol. Chem, 1994, 269, 2118–2124. [PubMed: 8294465]
16. Pettit GR; Herald CL; Doubek DL; Herald DL; Arnold E; Clardy J Isolation and structure of bryostatin 1. J. Am. Chem. Soc, 1982, 104, 6846–6848.
17. Sun MK; Hongpaisan J; Lim CS; Alkon DL Bryostatin-1 restores hippocampal synapses and spatial learning and memory in adult fragile x mice. J. Pharmacol. Exp. Ther, 2014, 349, 393–401. [PubMed: 24659806]
18. Kim H; Han SH; Quan HY; Jung YJ; An J; Kang P; Park JB; Yoon BJ; Seol GH; Min SS Bryostatin-1 promotes long-term potentiation via activation of PKCα and PKCε in the hippocampus. Neuroscience, 2012, 226, 348–355. [PubMed: 22986161]
19. Hongpaisan J; Xu C; Sen A; Nelson TJ; Alkon DL PKC activation during training restores mushroom spine synapses and memory in the aged rat. Neurobiol. Dis, 2013, 55, 44–62. [PubMed: 23545166]
20. Hongpaisan J; Alkon DL A structural basis for enhancement of long-term associative memory in single dendritic spines regulated by PKC. Proc. Natl. Acad. Sci. USA, 2007, 104, 19571–19576. [PubMed: 18073185]
21. Hongpaisan J; Sun MK; Alkon DL PKC ε activation prevents synaptic loss, Aβ elevation, and cognitive deficits in Alzheimer's disease transgenic mice. J. Neurosci, 2011, 31, 630–643. [PubMed: 21228172]
22. Sun MK; Alkon DL Dual effects of bryostatin-1 on spatial memory and depression. Eur. J. Pharmacol, 2005, 512, 43–51. [PubMed: 15814089]
23. Sun MK; Hongpaisan J; Alkon DL Rescue of Synaptic Phenotypes and Spatial Memory in Young Fragile X Mice. J. Pharmacol. Exp. Ther, 2016, 357, 300–310. [PubMed: 26941170]
24. Sun MK; Hongpaisan J; Nelson TJ; Alkon DL Poststroke neuronal rescue and synaptogenesis mediated in vivo by protein kinase C in adult brains. Proc. Natl. Acad. Sci. USA, 2008, 105, 13620–13625. [PubMed: 18768786]
25. Sun MK; Hongpaisan J; Alkon DL Postischemic PKC activation rescues retrograde and anterograde long-term memory. Proc. Natl. Acad. Sci. USA, 2009, 106, 14676–14680. [PubMed: 19667190]
26. Etcheberrigaray R; Tan M; Dewachter I; Kuipéri C; Van der Auwera I; Wera S; Qiao L; Bank B; Nelson TJ; Kozikowski AP; Van Leuven F; Alkon DL Therapeutic effects of PKC activators in

Alzheimer's disease transgenic mice. Proc. Natl. Acad. Sci. USA, 2004, 101, 11141–11146. [PubMed: 15263077]

27. Farlow MR; Thompson RE; Wei LJ; Tuchman AJ; Grenier E; Crockford D; Wilke S; Benison J; Alkon DL A Randomized, Double-Blind, Placebo-Controlled, Phase II Study Assessing Safety, Tolerability, and Efficacy of Bryostatin in the Treatment of Moderately Severe to Severe Alzheimer's Disease. J. Alzheimers Dis, 2019, 67, 555–570. [PubMed: 30530975]
28. Nelson TJ; Sun MK; Lim C; Sen A; Khan T; Chirila FV; Alkon DL Bryostatin Effects on Cognitive Function and PKCε in Alzheimer's Disease Phase IIa and Expanded Access Trials. J. Alzheimers Dis, 2017, 58, 521–535. [PubMed: 28482641]
29. Wender PA; Hardman CT; Ho S; Jeffreys MS; Maclaren JK; Quiroz RV; Ryckbosch SM; Shimizu AJ; Sloane JL; Stevens MC Scalable synthesis of bryostatin 1 and analogs, adjuvant leads against latent HIV. Science, 2017, 358, 218–223. [PubMed: 29026042]
30. Wager TT; Hou X; Verhoest PR; Villalobos A Central Nervous System Multiparameter Optimization Desirability: Application in Drug Discovery. ACS Chem. Neurosci. 2016, 7, 767–775. [PubMed: 26991242]
31. Zhang X; Zhang R; Zhao H; Cai H; Gush KA; Kerr RG; Pettit GR; Kraft AS Preclinical pharmacology of the natural product anticancer agent bryostatin 1, an activator of protein kinase C. Cancer Res, 1996, 56, 802–808. [PubMed: 8631017]
32. Nelson TJ; Sen A; Alkon DL; Sun MK Adduct formation in liquid chromatography-triple quadrupole mass spectrometric measurement of bryostatin 1. J. Chromatogr. B Analyt. Technol. Biomed. Life Sci, 2014, 944, 55–62.
33. Wender PA; Hinkle KW; Koehler MF; Lippa B The rational design of potential chemotherapeutic agents: synthesis of bryostatin analogues. Med. Res. Rev, 1999, 19, 388–407. [PubMed: 10502742]
34. Wender PA; Baryza JL; Bennett CE; Bi FC; Brenner SE; Clarke MO; Horan JC; Kan C; Lacôte E; Lippa B; Nell PG; Turner TM The practical synthesis of a novel and highly potent analogue of bryostatin. J. Am. Chem. Soc, 2002, 124, 13648–13649. [PubMed: 12431074]
35. DeChristopher BA; Fan AC; Felsher DW; Wender PA "Picolog," a synthetically-available bryostatin analog, inhibits growth of MYC-induced lymphoma in vivo. Oncotarget, 2012, 3, 58–66. [PubMed: 22308267]
36. Wender PA; Nakagawa Y; Near KE; Staveness D Computer-guided design, synthesis, and protein kinase C affinity of a new salicylate-based class of bryostatin analogs. Org. Lett, 2014, 16, 5136–5139. [PubMed: 25238583]
37. Wender PA; Baryza JL; Brenner SE; DeChristopher BA; Loy BA; Schrier AJ; Verma VA Design, synthesis, and evaluation of potent bryostatin analogs that modulate PKC translocation selectivity. Proc. Natl. Acad. Sci. USA, 2011, 108, 6721–6726. [PubMed: 21415363]
38. DeChristopher BA; Loy BA; Marsden MD; Schrier AJ; Zack JA; Wender PA Designed, synthetically accessible bryostatin analogues potently induce activation of latent HIV reservoirs in vitro. Nat. Chem, 2012, 4, 705–710. [PubMed: 22914190]
39. Wender PA; Staveness D Improved protein kinase C affinity through final step diversification of a simplified salicylate-derived bryostatin analog scaffold. Org. Lett, 2014, 16, 5140–5143. [PubMed: 25238640]
40. Staveness D; Abdelnabi R; Near KE; Nakagawa Y; Neyts J; Delang L; Leyssen P; Wender PA Inhibition of Chikungunya Virus-Induced Cell Death by Salicylate-Derived Bryostatin Analogues Provides Additional Evidence for a PKC-Independent Pathway. J. Nat. Prod, 2016, 79, 680–684. [PubMed: 26900711]
41. Staveness D; Abdelnabi R; Schrier AJ; Loy BA; Verma VA; DeChristopher BA; Near KE; Neyts J; Delang L; Leyssen P; Wender PA Simplified Bryostatin Analogues Protect Cells from Chikungunya Virus-Induced Cell Death. J. Nat. Prod, 2016, 79, 675–679. [PubMed: 26900625]
42. Santuy A; Rodríguez JR; DeFelipe J; Merchán-Pérez A Study of the Size and Shape of Synapses in the Juvenile Rat Somatosensory Cortex with 3D Electron Microscopy. eNeuro, 2018, 5, pii: ENEURO.0377–172017. doi: 10.1523/ENEURO.0377-17.2017.
43. Schätzle P; Wuttke R; Ziegler U; Sonderegger P Automated quantification of synapses by fluorescence microscopy. J. Neurosci. Methods, 2012, 204, 144–149. [PubMed: 22108140]

44. Dzyubenko E; Rozenberg A; Hermann DM; Faissner A Colocalization of synapse marker proteins evaluated by STED-microscopy reveals patterns of neuronal synapse distribution in vitro. J. Neurosci. Methods, 2016, 273, 149–159. [PubMed: 27615741]
45. Nieland TJ; Logan DJ; Saulnier J; Lam D; Johnson C; Root DE; Carpenter AE; Sabatini BL High content image analysis identifies novel regulators of synaptogenesis in a high-throughput RNAi screen of primary neurons. PLoS One, 2014, 9, e91744. [PubMed: 24633176]
46. Verstraelen P; Van Dyck M; Verschuuren M; Kashikar ND; Nuydens R; Timmermans JP; De Vos WH Image-Based Profiling of Synaptic Connectivity in Primary Neuronal Cell Culture. Front. Neurosci, 2018, 12, 389. [PubMed: 29997468]
47. Ippolito DM; Eroglu C Quantifying synapses: an immunocytochemistry-based assay to quantify synapse number. J. Vis. Exp, 2010, 45, pii: 2270. doi: 10.3791/2270.
48. Hoon M; Sinha R; Okawa H Using Fluorescent Markers to Estimate Synaptic Connectivity In Situ. Methods Mol. Biol, 2017, 1538, 293–320. [PubMed: 27943198]
49. Dani A; Huang B; Bergan J; Dulac C; Zhuang X Superresolution imaging of chemical synapses in the brain. Neuron, 2010, 68, 843–856. [PubMed: 21144999]
50. Burette A; Collman F; Micheva KD; Smith SJ; Weinberg RJ Knowing a synapse when you see one. Front. Neuroanat, 2015, 9, 100. [PubMed: 26283929]
51. Bleckert A; Parker ED; Kang Y; Pancaroglu R; Soto F; Lewis R; Craig AM; Wong RO Spatial relationships between GABAergic and glutamatergic synapses on the dendrites of distinct types of mouse retinal ganglion cells across development. PLoS One, 2013, 8, e69612. [PubMed: 23922756]
52. El-Husseini AE; Schnell E; Chetkovich DM; Nicoll RA; Bredt DS PSD-95 involvement in maturation of excitatory synapses. Science, 2000, 290, 1364–1368. [PubMed: 11082065]
53. Matthews SA; Pettit GR; Rozengurt E Bryostatin 1 induces biphasic activation of protein kinase D in intact cells. J. Biol. Chem, 1997, 272, 20245–20250. [PubMed: 9242703]
54. Lorenzo PS; Bögi K; Hughes KM; Beheshti M; Bhattacharyya D; Garfield SH; Pettit GR; Blumberg PM Differential roles of the tandem C1 domains of protein kinase C delta in the biphasic down-regulation induced by bryostatin 1. Cancer Res, 1999, 59, 6137–6144. [PubMed: 10626804]
55. Isakov N; Galron D; Mustelin T; Pettit GR; Altman A Inhibition of phorbol ester-induced T cell proliferation by bryostatin is associated with rapid degradation of protein kinase C. J. Immunol, 1993, 150, 1195–1204. [PubMed: 8432975]
56. Lee HW; Smith L; Pettit GR; Smith JB Bryostatin 1 and phorbol ester down-modulate protein kinase C-alpha and -epsilon via the ubiquitin/proteasome pathway in human fibroblasts. Mol. Pharmacol, 1997, 51, 439–447. [PubMed: 9058599]
57. Marsden MD; Loy BA; Wu X; Ramirez CM; Schrier AJ; Murray D; Shimizu A; Ryckbosch SM; Near KE; Chun TW; Wender PA; Zack JA In vivo activation of latent HIV with a synthetic bryostatin analog effects both latent cell “kick” and “kill” in strategy for virus eradication. PLoS Pathog., 2017, 13(9):e1006575. [PubMed: 28934369]
58. Dimitrijević SM; Ryves WJ; Parker PJ; Evans FJ Characterization of phorbol ester binding to protein kinase C isotypes. Mol. Pharmacol, 1995, 48, 259–267. [PubMed: 7651359]
59. Beans EJ; Fournogerakis D; Gauntlett C; Heumann LV; Kramer R; Marsden MD; Murray D; Chun TW; Zack JA; Wender PA Highly potent, synthetically accessible prostratin analogs induce latent HIV expression in vitro and ex vivo. Proc. Natl. Acad. Sci. USA, 2013, 110, 11698–11703. [PubMed: 23812750]
60. Olson DE Psychoplastogens: A Promising Class of Plasticity-Promoting Neurotherapeutics. J. of Exp. Neurosci, 2018, 12, 1–4.
61. Sen A; Hongpaisan J; Wang D; Nelson TJ; Alkon DL Protein Kinase Cϵ (PKCϵ) Promotes Synaptogenesis through Membrane Accumulation of the Postsynaptic Density Protein PSD-95. J. Biol. Chem, 2016, 291, 16462–16476. [PubMed: 27330081]
62. Staveness D Highly-simplified, Functional Bryostatin Analogs Through Design and Efforts Toward a Biorelevant Model for Allosteric Regulation of Protein Kinase C. Doctoral dissertation, Stanford University, Stanford, CA, 2015.

63. Sloane JL A Supply-impacting Synthesis of Clinical Lead Bryostatin 1 and the Design, Synthesis and Evaluation of Novel Protein Kinase C Modulators as Preclinical Leads. Doctoral dissertation, Stanford University, Stanford, CA, 2019.
64. Olson DE; Sleiman SF; Bourassa MW; Wagner FF; Gale JP; Zhang Y-L; Ratan RR; Holson EB Hydroxamate-based Histone Deacetylase Inhibitors Can Protect Neurons from Oxidative Stress by Forming Catalase Mimetic Complexes with Intracellular Iron. Chem. Biol, 2015, 22, 439–445. [PubMed: 25892200]
65. Sleiman SF; Olson DE; Bourassa MW; Karuppagounder SS; Zhang Y-L; Gale J; Wagner FF; Basso M; Coppola G; Pinto JT; Holson EB; Ratan RR Hydroxamic Acid-based Histone Deacetylase (HDAC) Inhibitors Can Mediate Neuroprotection Independent of HDAC Inhibition. J. Neurosci, 2014, 34, 14328–14337. [PubMed: 25339746]
66. Gschwendt M; Dieterich S; Rennecke J; Kittstein W; Mueller HJ; Johannes FJ Inhibition of protein kinase C mu by various inhibitors. Differentiation from protein kinase c isoenzymes. FEBS Lett, 1996, 392, 77–80. [PubMed: 8772178]
67. Larsson C Protein kinase C and the regulation of the actin cytoskeleton. Cell Signal, 2006, 18, 276–84. [PubMed: 16109477]
68. Schaffer TB; Smith JE; Cook EK; Phan T; Margolis SS PKCε Inhibits Neuronal Dendritic Spine Development through Dual Phosphorylation of Ephexin5. Cell Rep, 2018, 25, 2470–2483. [PubMed: 30485813]
69. Ly C; Greb AC; Cameron LP; Wong JM; Barragan EV; Wilson PC; Burbach KF; Soltanzadeh Zarandi S; Sood A; Paddy MR; Duim WC; Dennis MY; McAllister AK; Ori-McKenney KM; Gray JA; Olson DE Psychedelics Promote Structural and Functional Neural Plasticity. Cell Rep, 2018, 23, 3170–3182. [PubMed: 29898390]
70. Li N; Lee B; Liu RJ; Banasr M; Dwyer JM; Iwata M; Li XY; Aghajanian G; Duman RS mTOR-dependent synapse formation underlies the rapid antidepressant effects of NMDA antagonists. Science, 2010, 329, 959–964. [PubMed: 20724638]
71. Moda-Sava RN; Murdock MH; Parekh PK; Fetcho RN; Huang BS; Huynh TN; Witztum J; Shaver DC; Rosenthal DL; Always EJ; Lopez K; Meng Y; Nellissen L; Grosenick L; Milner TA; Deisseroth K; Bito H; Kasai H; Liston C Sustained rescue of prefrontal circuit dysfunction by antidepressant-induced spine formation. Science, 2019, 364, pii: eaat8078. [PubMed: 31624212]
72. Castrén E; Antila H Neuronal plasticity and neurotrophic factors in drug responses. Mol. Psychiatry, 2017, 22, 1085–1095 [PubMed: 28397840]
73. Li D; Hérault K; Silm K; Evrard A; Wojcik S; Oheim M; Herzog E; Ropert N Lack of evidence for vesicular glutamate transporter expression in mouse astrocytes. J. Neurosci, 2013, 33, 4434–4455. [PubMed: 23467360]
74. Won S; Incontro S; Nicoll RA; Roche KW PSD-95 stabilizes NMDA receptors by inducing the degradation of STEP61. Proc. Natl. Acad. Sci. USA, 2016, 113, E4736–44. [PubMed: 27457929]
75. Dunlap LE; Azinfar A; Ly C; Cameron LP; Viswanathan J; Tombari RJ; Myers-Turnbull D; Taylor JC; Grodzki AC; Lein PJ; Kokel D; Olson DE Identification of Psychoplastogenic N,N-Dimethylaminoisotryptamine (isoDMT) Analogs Through Structure-Activity Relationship Studies. J. Med. Chem, 2020, 63, 1142–1155.

A

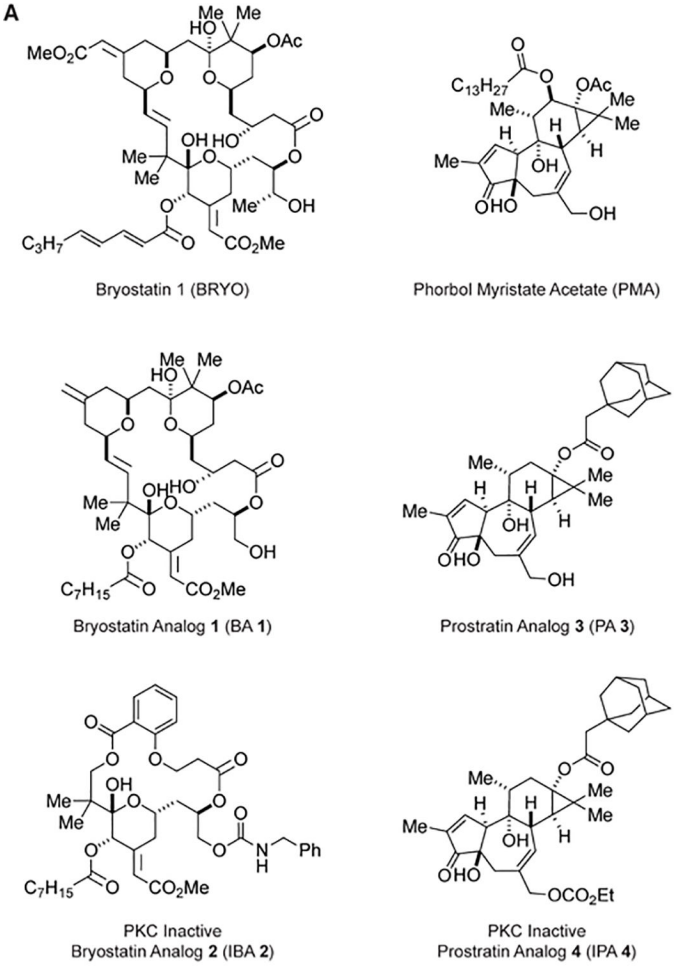

B

	PKCα	PKCβI	PKCγ	PKCδ	PKCε	PKCη	PKCθ
BRYO	0.81 (0.6–1.1)	2.2 (1.2–4.0)	2.2 (1.5–3.3)	2.1 (1.2–3.5)	3.0 (2.1–4.2)	2.2 (1.5–3.2)	1.5 (1.0–2.1)
BA **1**	1.8 (1.1–2.9)	6.3 (3.5–11)	5.6 (3.0–10)	2.0 (1.3–3.0)	5.8 (2.3–12)	6.4 (3.6–11)	2.0 (1.1–3.6)
IBA **2**	>5000	>5000	ND	>5000	>5000	ND	ND
PMA	1.5	3.54	17.39	1.61	9.04	ND	ND
PA **3**	1.4 (0.88–2.2)	3.1 (2.0–4.8)	1.9 (1.3–2.9)	0.51 (0.35–0.75)	1.7 (1.1–2.6)	1.9 (1.3–2.9)	1.6 (0.88–2.8)
IPA **4**	460 (260–820)	480 (240–930)	ND	380 (230–630)	300 (200–440)	ND	ND

Figure 1. Chemical tools for studying the effects of PKC modulation on neuronal structure.

(A) Chemical structures of compounds used in this study. Unlike BRYO, BA **1**, PMA, and PA **3**, the inactive compounds IBA **2** and IPA **4** do not bind PKC and serve as structurally similar negative control compounds for bryostatin and prostratin analogs, respectively. (B) Ki values (nM) for various PKC isoforms determined using a cell free assay. Ranges in parentheses represent 95% confidence intervals. The values for BA **1** have been previously reported.[22] Values for PMA were calculated from previously reported data[23] using the Cheng-Prusoff equation. ND = not determined.

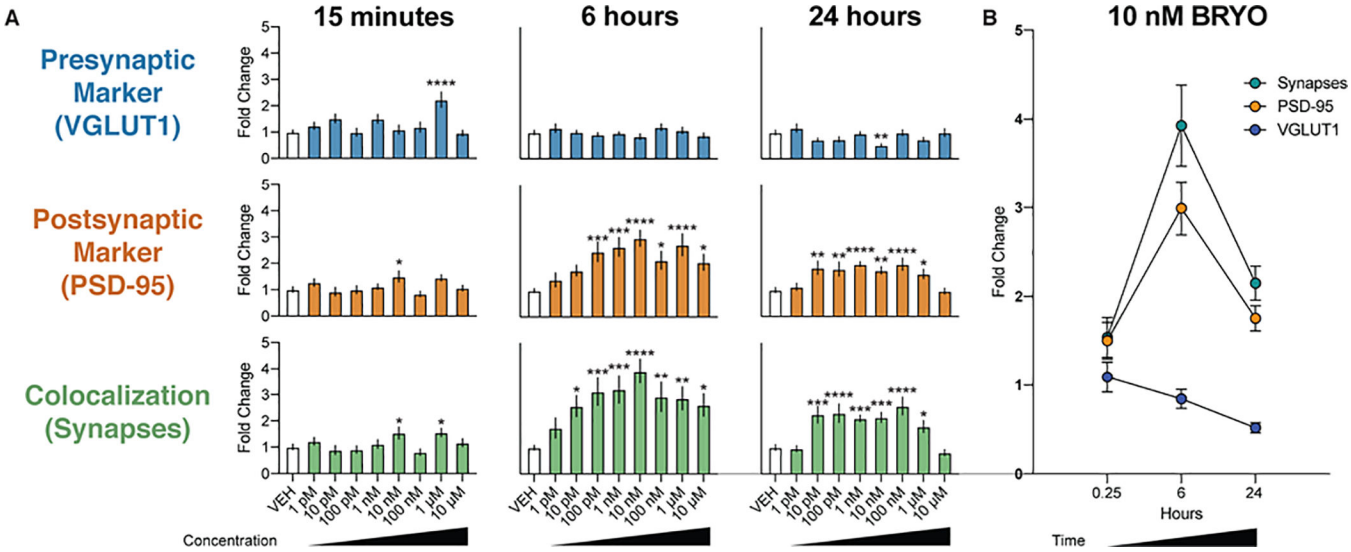

Figure 2. Bryostatin 1 increases synaptogenesis in cortical cultures.

(A) Time- and concentration-response studies demonstrate that BRYO increases PSD-95 and synapse density in an inverted U-shaped pattern. Maximal synaptic density was achieved following treatment with BRYO for 6 h at 10 nM (N = 16–50 neurons per condition). (B) BRYO (10 nM) increases synaptic density more than PSD-95 density. Data are represented as mean ± SEM. *p < 0.05, **p < 0.01, ***p < 0.001, ****p < 0.0001, as compared to vehicle control (one-way ANOVA with Dunnett's post hoc test). Statistics were not performed on the data in B. VEH = vehicle, KET = ketamine, treated at 10 µM

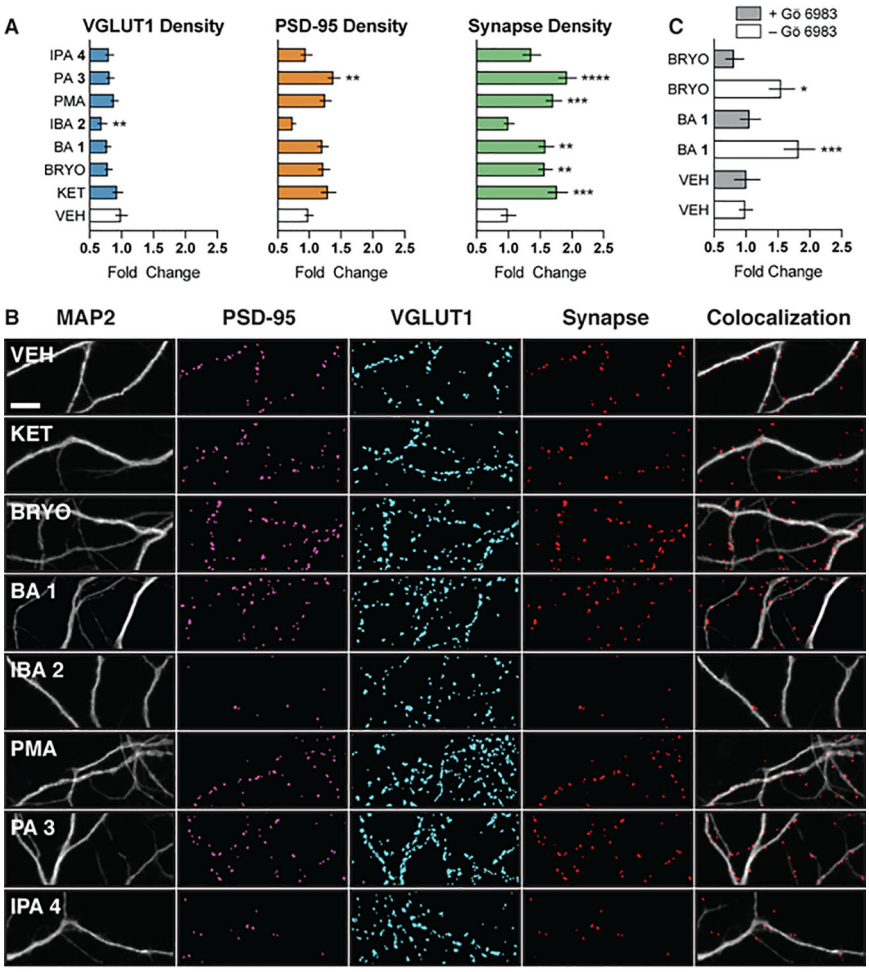

Figure 3. Bryostatin 1 increases synaptogenesis in cortical cultures through a PKC-dependent mechanism.

(A) PKC activators (BRYO, BA **1**, PMA, and PA **3**), but not inactive analogs (IBA **2** and IPA **4**), increase PSD-95 and synapse density in cortical cultures when treated for 6 h at 10 nM (N = 37–54 neurons per condition). (B) Representative images of cortical cultures (DIV19–20) treated with compounds for 6 h at 10 nM. Dendrites, presynaptic sites, and postsynaptic sites are labeled using antibodies for MAP2 (grey), PSD-95 (magenta), and VGLUT1 (cyan), respectively. Synapses (red) were identified by colocalization events of pre- and postsynaptic puncta meeting defined intensity and size requirements (see Methods). Scale bar = 10 μm. (C) The pan PKC inhibitor Gö 6983 (100 nM) blocks the ability of BRYO and BA **1** (6 h, 10 nM treatments) to promote synaptogenesis (N = 41–144 neurons per condition). Data are represented as mean ± SEM. *p < 0.05, **p < 0.01, ***p < 0.001, ****p < 0.0001, as compared to vehicle control (one-way ANOVA with Dunnett's post hoc test). VEH = vehicle, KET = ketamine, treated at 10 μM.

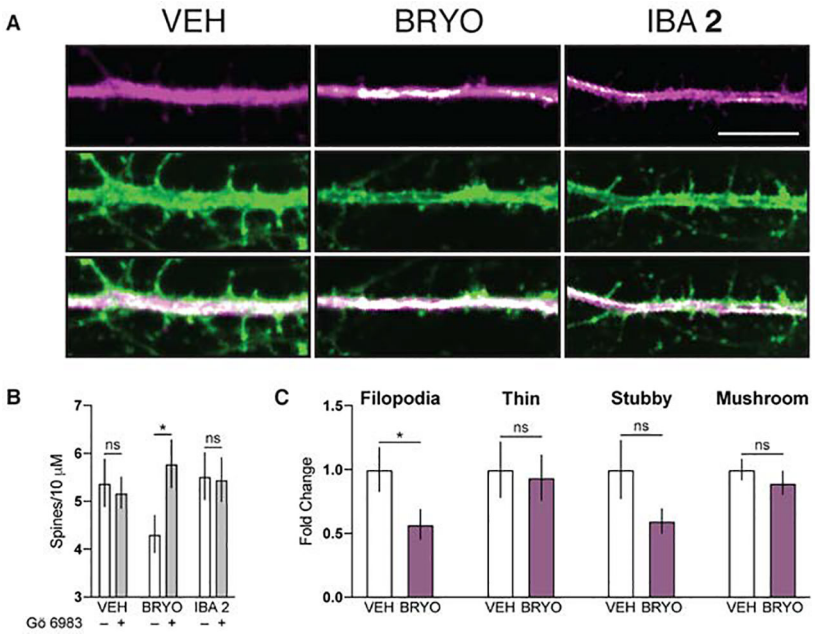

Figure 4. Bryostatin 1 decreases dendritic spine density in cortical cultures through a PKC-dependent mechanism.

(A) Representative images of cortical cultures (DIV20–21) treated with BRYO or IBA **2** for 6 h at 10 nM. Dendrites were labeled using an antibody against MAP2 (magenta), and F-actin was labeled with a fluorescent phalloidin conjugate (green). When the two channels are overlaid, dendritic spines can be identified as green protrusions extending beyond the magenta dendrites. Scale bar = 5 µm. (B) Quantification of dendritic spine density in the absence (–) and presence (+) of the pan PKC inhibitor Gö 6983. (C) Quantification of dendritic spine type. N = 21–24 neurons per condition. Data are represented as mean ± SEM. *$p < 0.05$ (Student's t-test). VEH = vehicle.

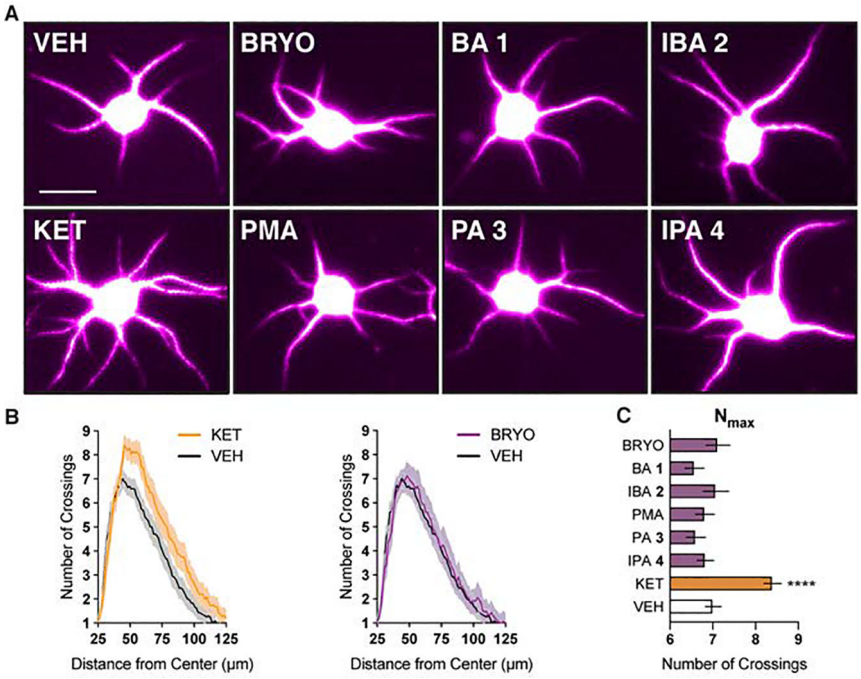

Figure 5. Bryostatin 1 does not influence dendritic arbor complexity in cortical cultures.

(A) Representative images of cortical cultures (DIV6) treated with compounds for 6 h at 10 nM. Dendrites were labeled using an antibody against MAP2 (magenta). Scale bar = 20 μm. (B) Representative Sholl plots demonstrate that ketamine, but not BRYO, increases the complexity of dendritic arbors. Shadings indicated 95% confidence intervals. (C) The N_{max} values of the Sholl plots demonstrate that BRYO and related PKC activators do not increase dendritic arbor complexity (N = 81–107 neurons per condition). Data are represented as mean ± SEM. ****$p < 0.0001$, as compared to vehicle control (one-way ANOVA with Dunnett's post hoc test). VEH = vehicle, KET = ketamine, treated at 10 μM.